Conference Paper, Published Version

Karmpadakis, Ioannis; Swan, Chris; Christou, Marios

Wave Height and Crest Height Distributions in Shallow Water: Analysis of Field Data

Coastal Structures 2019 - Nils Goseberg, Torsten Schlurmann (eds) - © 2019 Bundesanstalt für Wasserbau
ISBN 978-3-939230-64-9 (Online) - DOI: 10.18451/978-3-939230-64-9_064

Wave Height and Crest Height Distributions in Shallow Water: Analysis of Field Data

I. Karmpadakis, C. Swan & M. Christou
Imperial College London, United Kingdom

Abstract: This paper presents an analysis of field measurements obtained at an offshore platform in the Southern North Sea. These measurements are used to examine the accuracy of a wide range of wave height and crest height statistical models. More specifically, the available field data are used to define the model that provides the best description for a broad range of incident wave conditions; the latter corresponding to conditions arising in the shallow end of the intermediate water depth regime. Additionally, the primary sources of the discrepancies are investigated, and guidance is provided for the selection of appropriate models. Taken together, the results presented herein provide insights as to the importance of physical mechanisms such as wave breaking, and have significant implications in the selection of appropriate design parameters.

Keywords: wave heights, crest heights, shallow water, field data, wave breaking, short-term distribution

1 Introduction

Recent growth in the offshore wind energy sector has regenerated engineering interest in the design of marine structures. A crucial part of this process involves the calculation of the appropriate incident wave conditions. However, these calculations can turn out to be particularly challenging as the water depth reduces. Enhanced non-linear wave-wave interactions, depth limitations, wind and current effects are only a few examples that demonstrate the complexity of the processes involved in intermediate and shallow water depths.

In addressing this challenge, an extensive collection of surface elevation measurements from the Southern North Sea is examined. These measurements have been recorded by a wave radar, mounted on the side of an offshore platform; the instrumentation complying with the highest standards in wave measurements. Additionally, strict quality control procedures were applied to provide the best possible quality in the final dataset. Using these results, we present an insightful analysis of important wave characteristics. The primary focus of this analysis lies in the investigation of the short-term wave height and crest height distributions. Their behaviour is examined under a wide variety of incident sea-state conditions. These cover a broad range of effective water depths (around the shallow end of intermediate water) and a wide variety of sea-state steepnesses. Using the full range of available data, physical insights on the influence of important parameters are provided. In principle, these are related to the effects of non-linearity, reduced water depth and spectral bandwidth; particular attention being paid to their relation with the non-linear changes in the surface elevation and wave breaking. Finally, a large number of existing statistical models are assessed. Following an objective error quantification, suggestions are provided regarding the applicability of these models. Moreover, the best performing models, under a variety of sea-state conditions, are noted and explained.

Taken together, these results provide significant insights into the statistical distributions of wave heights and crest heights in intermediate and shallow water depths. Moreover, the present analysis

provides guidance towards the important physical mechanisms and the models that can accurately describe them. The implications of these findings extend to many aspects of engineering design; one example being the selection of an appropriate design wave for the calculation of wave forcing. This becomes particularly important when considering the magnitude of the discrepancies between the range of existing models and the measured data.

2 Background

Several short-term statistical models have been proposed in the literature; the aim being to provide an accurate description of the distribution of either the wave heights or crest heights. This section briefly presents the functional forms of some of the most commonly applied models in engineering design. These models are subsequently assessed using the available data in Section 4.

2.1 Wave height distributions

The short-term distribution of wave heights is defined by $Q(H)$, where Q is the probability of exceedance and H the wave height. The models considered herein are sub-divided into two categories: "deep-water" (2.1.1-2.1.4) and "shallow-water" (2.1.5-2.1.7) distributions based on whether the effects of depth-induced wave breaking are incorporated.

2.1.1 Rayleigh distribution (Longuet-Higgins, 1952)

$$Q(H) = \exp\left(-\frac{H^2}{8\sigma_\eta^2}\right), \tag{1}$$

where $\sigma_\eta$is the standard deviation of the free surface elevation. Based on the assumption of a linear but narrow-banded representation of a sea-state, this model is known to overpredict measured wave heights in realistic conditions.

2.1.2 Forristall distribution (Forristall, 1978)

$$Q(H) = \exp\left[-\frac{1}{\beta}\left(\frac{H}{\sigma_\eta}\right)^\alpha\right], \tag{2}$$

where $\alpha = 2.126$ and $\beta = 8.42$. This model is an empirical fit to wave measurements in intermediate water depths and has been well validated with measurements in the North Sea.

2.1.3 Naess distribution (Naess, 1985)

$$Q(H) = \exp\left[-\frac{1}{4\left(1-r\left(\frac{T}{2}\right)\right)}\left(\frac{H}{\sigma_\eta}\right)^2\right], \tag{3}$$

where $r(\tau) = \frac{\int_0^\infty S_{\eta\eta}\cos(\omega\tau)\mathrm{d}\omega}{\sigma_\eta^2}$ is the normalized autocorrelation function and the period T is obtained from the first minimum of the autocorrelation function (Tayfun and Fedele, 2007). In considering this solution, it is worth noting that in the narrow-banded limit $\left[r\left(\frac{T}{2}\right) = -1\right]$, it reduces to the Rayleigh distribution.

2.1.4 Boccotti distribution (Boccotti, 1989)

$$Q(H) = 1 + \frac{\ddot{r}(T)}{\sqrt{2\dot{r}(T)\left(1-r(T)\right)}}\exp\left[-\frac{1}{4\left(1-r\left(\frac{T}{2}\right)\right)}\left(\frac{H}{\sigma_\eta}\right)^2\right], \tag{4}$$

where T and $r(\tau)$ are as defined above and the double over-dot denotes a second time derivative. It should be mentioned that the Boccotti distribution is an asymptotic model, appropriate to large wave heights ($H \to H_{\max}$), and, as such, the integral of its probability density function does not equal unity.

2.1.5 Glukhovskiy-type distributions (Glukhovskiy, 1966)

$$Q(H) = \exp\left[-A\left(\frac{H}{H_m}\right)^K\right], \tag{5}$$

where the scale parameter, A, and shape parameter, K, are given by:

$$A = \frac{\pi}{4}\frac{1}{\left(1+\frac{\frac{H_m}{d}}{\sqrt{2\pi}}\right)} \quad , \quad K = \frac{2}{\left(1-\frac{H_m}{d}\right)}, \quad \text{where} \quad H_m \quad \text{is the mean wave height.} \tag{6}$$

In this form, the Glukhovskiy model cannot be applied without prior knowledge of H_m. As such, it cannot be used in a predictive manner. To overcome this issue, two alternative versions of the Glukhovskiy distribution are examined. The first, proposed by van Vledder (1991), uses an iterative scheme to estimate H_m from the root-mean-square wave height (H_{rms}). With Γ the incomplete gamma function and ϵ_s a predefined error ($O{\sim}10^{-6}$), the solution is defined by:

$$K^i = \frac{2}{\left(1-\frac{H_m^i}{d}\right)} \quad , \quad H_m^{i+1} = H_{\mathrm{rms}}\frac{\Gamma\left(\frac{1}{K^i}+1\right)}{\sqrt{\Gamma\left(\frac{2}{K^i}+1\right)}} \quad \text{until} \quad \left|H_m^{i+1} - H_m^i\right| < \epsilon_s \quad \text{and} \quad A = \left[\Gamma\left(\frac{2}{\mathrm{K}}+1\right)\right]^{\frac{K}{2}} \tag{7}$$

The second model was proposed by Klopman (1996) and its functional form is given by:

$$Q(H) = \exp\left[-A\left(\frac{H}{H_{\mathrm{rms}}}\right)^K\right], \quad \text{with} \quad K = \frac{2}{\left(1-0.7\frac{H_{\mathrm{rms}}}{d}\right)} \quad \text{and } A \text{ as above.} \tag{8}$$

2.1.6 Battjes-Groenendijk distribution (Battjes and Groenendijk, 2000)

$$Q(H) = \begin{cases} \exp\left[-\left(\frac{H}{H_1}\right)^2\right] & \text{for } H \le H_{tr} \\ \exp\left[-\left(\frac{H}{H_2}\right)^{3.6}\right] & \text{for } H > H_{tr} \end{cases} \quad \text{with} \quad H_{tr} = (0.35 + 5.8\tan\alpha\,)d \tag{9}$$

where $\tan\alpha$ is the bed slope, and H_1 and H_2 can be obtained from Table 2 of the paper. In effect, this model is a two-part Weibull distribution assuming a Rayleigh form for wave heights below the transitional H_{tr} and an empirical fit for the largest waves. In the first instance, the empirical coefficients have been obtained from uni-directional laboratory experiments. More recently, modifications based on field data have been proposed by Mai et al. (2011).

2.1.7 Mendez distribution Mendez et al. (2004)

$$Q(H) = \exp\left[-\phi^2(\kappa)\left(\frac{\xi}{1-\kappa\xi}\right)^2\right], \quad \text{with} \quad \xi = \frac{H}{H_{\mathrm{rms}}},\ \phi(\kappa) = (1-\kappa^{0.944})^{1.1877} \tag{10}$$

and κ being obtained from experimental measurements as a function of the Irribaren number and H_{rms}/d. This model has been obtained by assuming an initial Rayleigh distribution in deep water and incorporating shoaling and wave breaking using a bore approach (Battjes & Janssen, 1978).

2.2 Crest height distributions

Two crest height models have been considered in the present study. Both can be expressed as:

$$Q(\eta_c) = \exp\left[-\alpha\left(\frac{\eta_c}{H_s}\right)^\beta\right] \tag{11}$$

where η_c are the crest heights and H_s the significant wave height. The well-known Rayleigh distribution is obtained for $\alpha = 8$ and $\beta = 2$. Since this model is based on linear and narrow-banded assumptions, it is known to under-estimate the largest crest heights. The second model, proposed by Forristall (2000), incorporates effects up to a second-order of wave steepness. This solution fits a Weibull distribution to numerical simulations based upon Sharma and Dean (1981), with the scale and shape parameters of the distribution defined as a function of mean sea-state steepness (S_1) and the Ursell number (Ur). This model is commonly adopted as recommended practice in engineering design (DNV, 2010). However, recent findings suggest that it could be under-estimating the largest crest heights by up to 10% in deep and intermediate water depths (Latheef and Swan, 2013; Karmpadakis et al., 2019). At the same time, since the model does not incorporate any effects of wave breaking, it is expected to provide conservative estimates for sea-states in shallow water.

3 Methods

The accuracy of the aforementioned statistical models has been assessed using water surface elevation measurements from the field. These were recorded at an offshore platform in the Southern North Sea located in a water depth of 8 m. The bottom bathymetry in the vicinity of the platform is characterized by a very mild slope ($m < 1/500$). The measuring period spans the years between 2007-2017; recordings prior to 2011 are segmental, while for the rest of the period continuous measurements were available.

The measurements analysed herein have been recorded by a wave radar (Saab Rex D) mounted on the side of the platform; a photograph of the sensor being shown in Figure 1. The wave radar was positioned 26.5 m above the mean water level and was clear from obstructions. This particular sensor is widely used for platform-based surface elevation measurements and can provide high quality recordings. Its sampling rate can be set between 1 to 10 Hz and has an angular microwave beam width of 10^{o}. Considering the present dataset, the vast majority of records were obtained with a sampling rate of 4 Hz; a subset being recorded at 2 Hz (measurements before 2012). A review of the wave radar's functionality and accuracy can be found in Ewans et al. (2014).

In terms of analysing the recorded data, the measured airgap was first inverted, and any tidal fluctuations or storm surges were removed. The resulting time-series were then passed through strict quality control (QC) procedures following the method of Christou and Ewans (2011). Effectively, by identifying a series of flags, different types of potential erroneous measurements were identified and discarded. The sea-states that passed the QC were then analysed using zero-crossing and spectral analysis techniques. The final database consists of approximately 111,000 20-minute sea-states including more than 33,000,000 individual waves. The number of sea-states that failed the QC procedures was approximately 19,000.

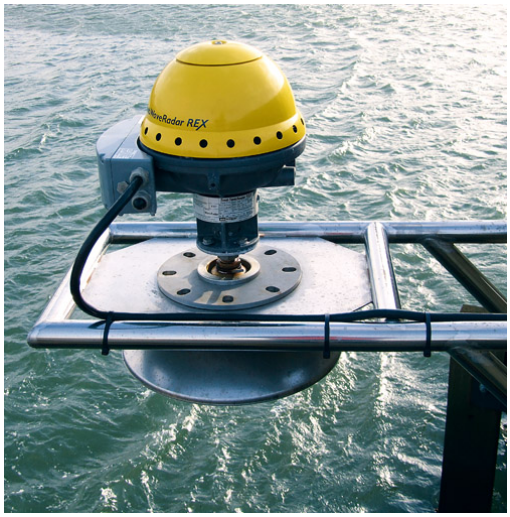

Fig. 1. Photograph of the Saab REX wave radar (Aqua, 2014).

Using this database, the existing statistical models were compared to the measured data. This was achieved by dividing the available sea-states into small subsets (or bins) with similar metocean characteristics. More specifically, the data bins presented herein were derived from the (H_s, T_p) parameter space with a bin size of 0.5 m in H_s and 1 s in T_p. To quantify the divergence between the predictions of each model and the recorded data within each data bin, an error metric was defined by:

$$\epsilon = \sqrt{\frac{1}{N}\sum_{i=p}^{N}\left(\frac{H_{meas}^{i}}{H_{model}^{i}} - 1\right)^2}, \tag{12}$$

where N is the number of zero-crossing waves, H_{meas}^{i} and H_{model}^{i} are the measured and predicted (modelled) wave heights. For each calculation the summation starts from the p^{th} observation corresponding to a given percentile of the order statistics and extends towards the smallest available probability of exceedance. The percentiles considered in the present work correspond to 20%, 10% and 1% $[P_{20}, P_{10}$ and $P_1]$. Adopting this approach, the P_{20} percentile examines the bulk of the distribution while the P_1 percentile concentrates on the tail of the distribution. This approach allows for the isolated assessment of the largest waves (or those arising at the tail of the distribution). These waves typically attract engineering interest defining the ULS or ALS design condition and are the first to be affected by wave breaking.

4 Results

4.1 Wave heights

By comparing the errors associated with the different models for each data bin, a map is obtained indicating the model that provides the best statistical description of wave heights. This is shown in Figure 2(a) with respect to the bulk of the distribution $[P_{20}]$ and Figure 2(b) for the tail of the distribution $[P_1]$. These results are illustrated in the non-dimensional parameter space $(H_s/d\,, k_p d)$ to provide a more general overview. It is clear from these results that none of the models provide the best statistical description across the whole range of effective water depths $(k_p d)$ and sea-state severities (H_s/d) irrespective of the chosen percentile. Moreover, with respect to the classification introduced in Section 2, there are only a few data bins in which the "deep-water" models provide the best fit. This is not unexpected since for the observed sea-state conditions and water depth, wave breaking has a significant impact on the wave height distribution.

In examining the performance of the shallow-water models for the bulk of the distribution, it can be seen that a pattern emerges. This relates to the best fit models as a function of H_s/d. For $H_s/d < 0.35$ the Glukhovskiy-type models provide the best fit; for $0.35 < H_s/d < 0.45$ the Mendez model is best while for $H_s/d > 0.45$ the Battjes-Groenendijk model. The explanation for this behaviour lies in the parametrisation adopted in each of these models for the incorporation of the dissipative effects of wave breaking. Specifically, the Glukhovskiy-type models are most appropriate for less severe sea-states, while the other two models better describe the more severe sea-states in reduced water depths. Indeed, both the Mendez and Battjes-Groenendijk distributions were derived to address shallow foreshores and were calibrated accordingly. In considering the results presented in Figure 2(b), it can be seen that the situation does not change significantly in the tail of the distribution. The main difference between the two sub-plots is the increased scatter for the P_1 probability level. This increased scatter is a consequence of the reduced number of observations in the tail of the distribution when compared to the main body of the data.

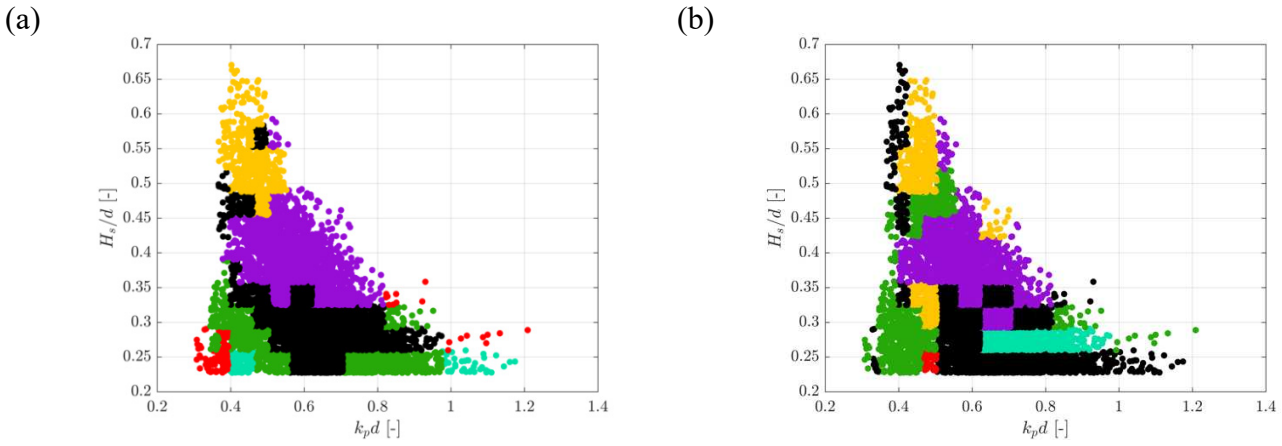

Fig. 2. Maps indicating the best fitting distribution for (a) the P_{20} [20%] and (b) the P_1 [1%] probability levels relating to the: Rayleigh [•], Forristall [•], Klopman [•], van Vledder [•], Battjes-Groenendijk [•], Mendez [•], Boccotti [•] and Naess [•] models. These results all relate to data recorded in a water depth of $d = 8$ m.

While the best fit maps provide clear guidance onto which models are most accurate in a variety of sea-states, it is instructive to examine the distribution of errors for some of the models considered. To this end, Figure 3 presents the error contours relating to 4 distributions mapped onto the (H_s, T_p) parameter space; the errors again being based on comparisons to the field data recorded in a water depth of $d = 8$ m. In Figure 3(a), the Rayleigh distribution is shown to exhibit large errors over the whole domain. This is not surprising since the model does not incorporate either wave breaking or any modifications for finite spectral bandwidth. Figure 3(b) shows results relating to the Boccotti distribution. In this case, the error levels are significantly reduced for moderate sea-states ($H_s \approx 2$ m), but increase around the periphery of the domain and for the steepest sea-states; the latter being dominated by wave breaking. The van Vledder model in Figure 3(c) exhibits similar behaviour. It could be argued that for some of the steep sea-states its performance is slightly improved due to the incorporation of wave breaking. Finally, the Battjes-Groenendijk model is considered in Figure 3(d). In this case, the opposite behaviour is observed. The steepest sea-states ($H_s > 3$ m) are now well modelled, while significant errors arise in the moderate sea-states. The reason for this behaviour lies in the two-part nature of this model. For the moderate sea-states the Battjes-Groenendijk model defaults to the Rayleigh distribution. Indeed, when comparing the errors associated with these two models in the lower part of the domain ($H_s < 2$ m), similar results arise.

The effects of sea-state steepness and spectral bandwidth are examined in Figures 4(a) and 4(b) respectively. Both sub-plots present the short-term distribution of normalised wave heights (H/H_s) arising in specific data bins. In Figure 4(a) the wave heights included in the data bin have been grouped with respect to the spectral bandwidth of the sea-state; the latter defined by:

$$\nu = \sqrt{\frac{m_0 m_2}{m_1^2} - 1}, \tag{13}$$

where $m_n = \int_0^\infty \omega^n S_{\eta\eta} \mathrm{d}\omega$ represent the spectral moments of order n. In considering these data, it is clear that an increase in the spectral bandwidth from $\nu = 0.45$ to $\nu = 0.6$ and $\nu = 0.7$ lead to a decorrelation between crests and troughs and consequently, to smaller wave heights. Moreover, it is important to note that the data bin corresponds to moderate sea-state conditions, $H_s/d \approx 0.2$, to avoid

the effects of wave breaking. This latter effect is illustrated in Figure 4(b). In this case, increases in the mean sea-state steepness from $S_1 = 0.025$ to $S_1 = 0.035$ and $S_1 = 0.04$ lead to a rapid reduction in the largest wave heights for ($k_p d = 0.6$). Considering the severity of these sea-states this effect is attributed to wave breaking.

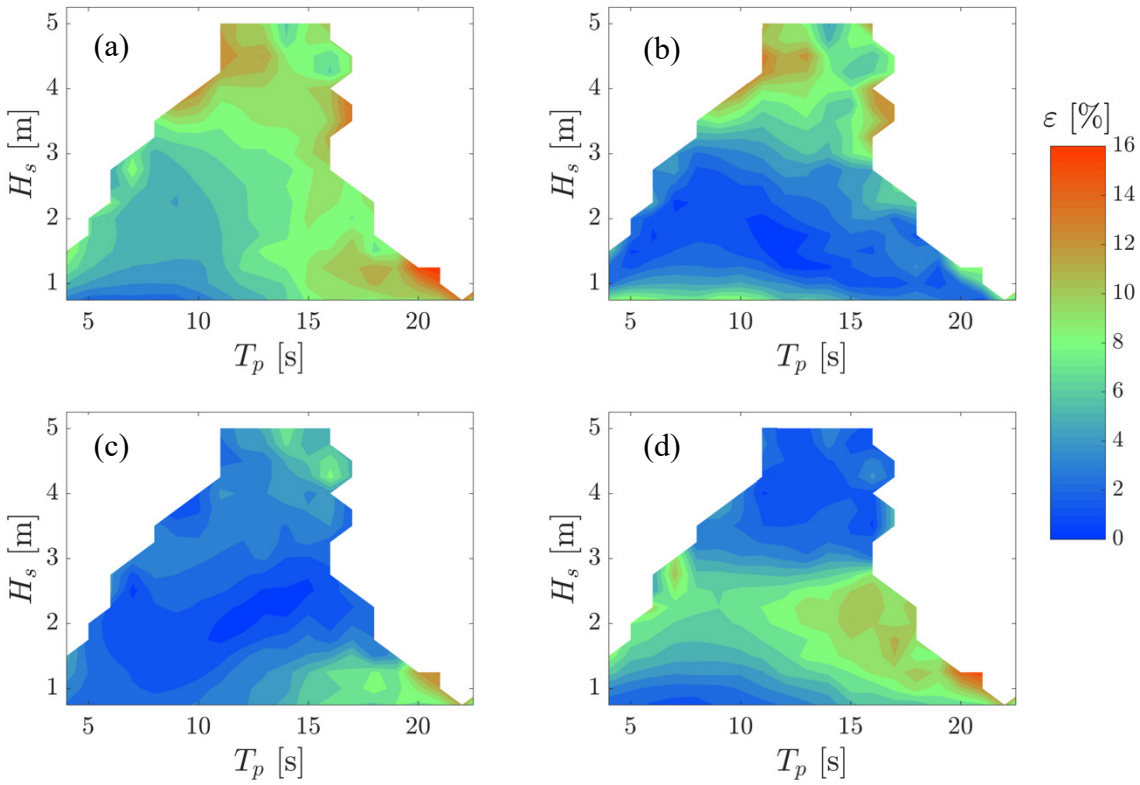

Fig. 3. Error contours between model predictions and field data recorded in a water depth of $d = 8$ m. The sub-plots correspond to the: (a) Rayleigh, (b) Boccotti, (c) van Vledder and (d) Battjes-Groenendijk models and the P_{10} percentile.

Taken together these results present the dependence of the short-term wave height distributions on spectral bandwidth and sea-state steepness. Considering how these are introduced in the statistical models, it is noted that the Boccotti and Naess models incorporate the effects of spectral bandwidth analytically. However, they do not incorporate wave breaking. In contrast, the "shallow-water" models primarily incorporate the effects of wave breaking through empirical parametrisations. These models, however, do not account for the effects of spectral bandwidth explicitly; some indirect dependence is, nonetheless, introduced through the parametric representation of H_{rms}. Since the Forristall model is a (single-parameter) fit to measured data, both effects are indirectly introduced, but the flexibility of the model is limited. Similar findings have been presented in Karmpadakis (2019) along with a detailed investigation of a significantly larger field database supplemented by extensive laboratory measurements; the latter explained in Karmpadakis et al. (2019).

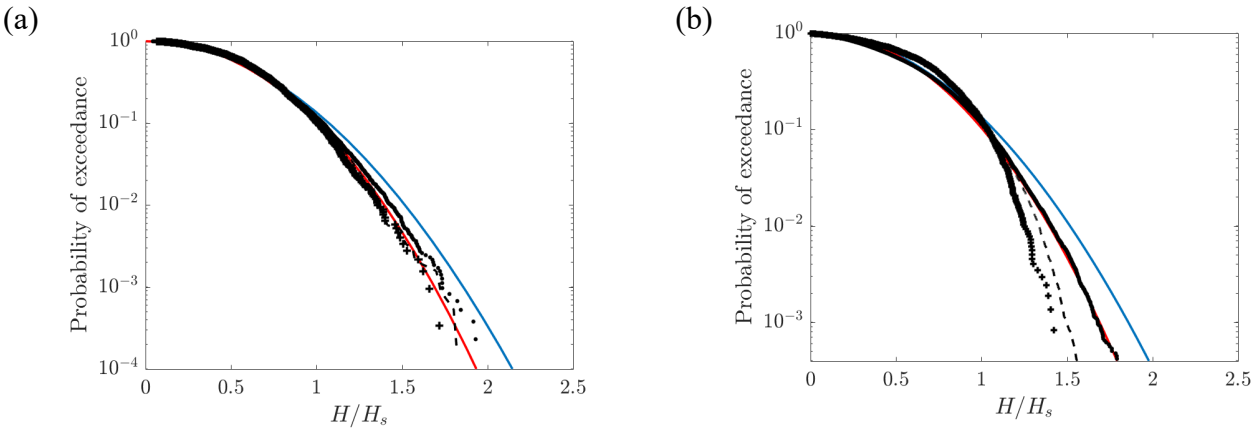

Fig. 4. Normalised wave height distributions showing the effects of (a) spectral bandwidth and (b) sea-state steepness. Sub-plot (a) relates to $(H_s/d = 0.2, k_p d = 0.5)$ and compares sea-states with $\nu = 0.45$[•], $\nu = 0.6$ [–] and $\nu = 0.7$[+]. Sub-plot (b) compares $S_1 = 0.025$[•], $S_1 = 0.035$ [– –] and $S_1 = 0.04$[+] for $k_p\, d = 0.6$. The Rayleigh [•] and Forristall [•] models have been added for reference; with all the data recorded in a water depth of $d = 8$ m.

4.2 *Crest heights*

Following a similar approach, the crest heights recorded in the field are compared to the models presented in Section 2. Since the Rayleigh distribution is well known to under-estimate the largest crest heights, the comparisons focus on the performance of the Forristall (2000) second-order model. In particular, the influence of the competing mechanisms of nonlinear amplifications (beyond second-order) and wave breaking are examined.

To this end, Figure 5 shows normalised crest height distributions (η_c/H_s) from selected data bins with comparisons to the predictions of the Rayleigh and Forristall models. The sub-plots have been arranged with increasing sea-state steepness to illustrate the effects of nonlinearity on the crest height distributions. As such, Figure 5(a) presents results relating to a data bin with moderate sea-states ($S_1 = 0.025$). These results confirm that whilst the Rayleigh model under-estimates the measurements, the Forristall model can accurately describe the measured data. In Figure 5(b) steeper sea-states are considered ($S_1 = 0.03$). In this case it is clear that amplifications beyond the Forristall model arise in the tail of the distribution. These are attributed to higher-order nonlinear interactions. While their occurrence has been well documented with respect to field, laboratory and numerical data in deep water, there are relatively few studies that demonstrate their existence in finite water depths (Karmpadakis et al.,2019).

Considering the steeper sea-states in Figures 5(c) and 5(d), a second mechanism appears to become increasingly important. This acts to reduce the largest crest heights lying at the tail of the distribution. Undoubtedly, this is caused by the dissipative effects of wave breaking. In fact, it can be seen that for the less steep case in Figure 5(c) with $S_1 = 0.034$, the reductions in the tail of the distribution are clear but not that extensive. However, for the steepest case in Figure 5(d) with $S_1 = 0.036$, the drop in

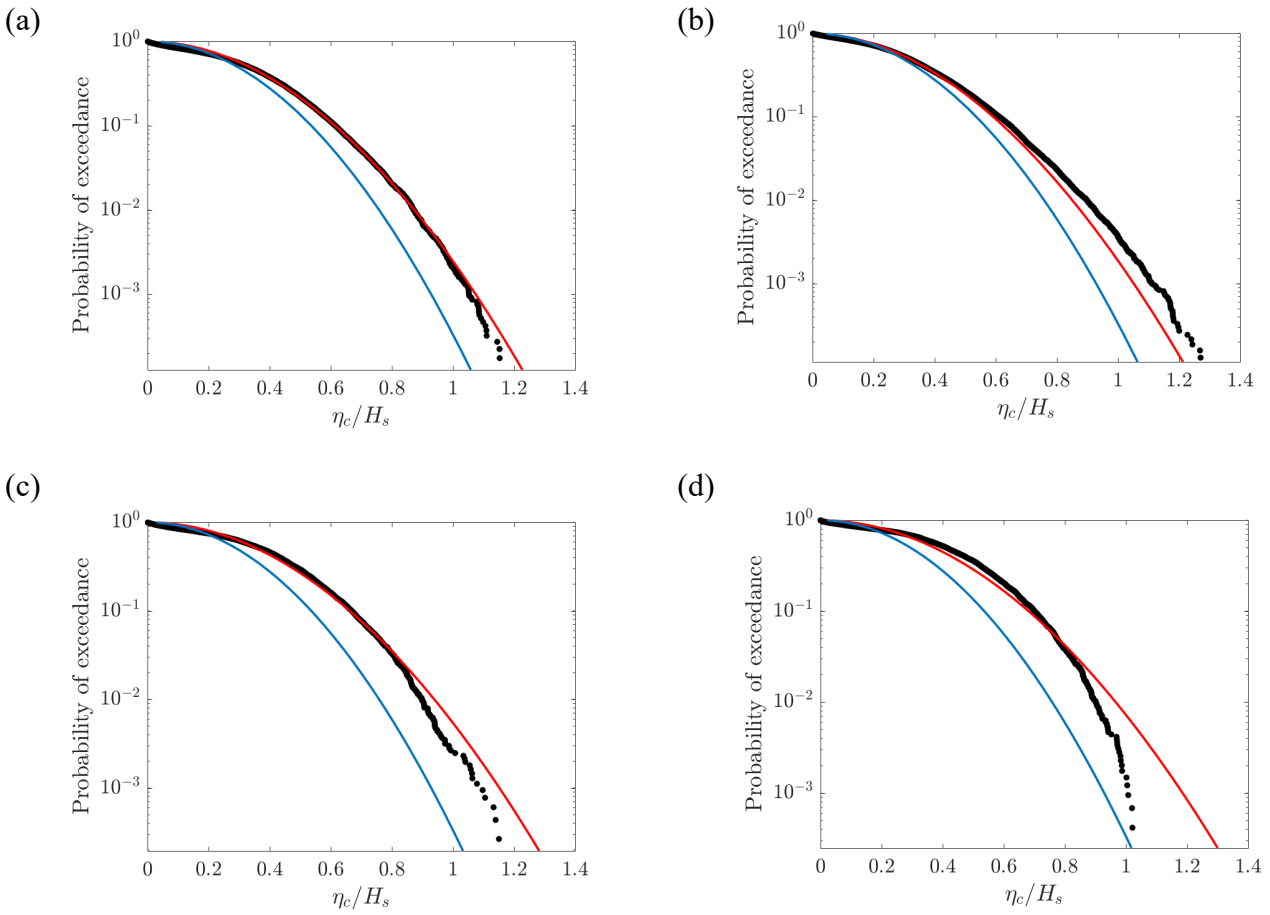

Fig. 5. Normalised crest height distributions (η_c/H_s) from data bins recorded in a water depth of $d = 8$ m, with comparisons to the Rayleigh [•] and Forristall [•] models. The sub-plots have been arranged with increasing steepness to show the effects of nonlinearity. The corresponding data bins are defined by: (a) $S_1 = 0.025$ ($H_s = 2.25$ m, $T_p = 12$ s), (b) $S_1 = 0.03$ ($H_s = 2$ m, $T_p = 9$ s), (c) $S_1 = 0.034$ ($H_s = 3.25$ m, $T_p = 13$ s) and (d) $S_1 = 0.036$ ($H_s = 4.5$ m, $T_p = 13$ s).

the tail of the distribution is significant. This is accompanied by an increase of smaller crest heights ($Q \approx 10^{-1}$) owing to the redistribution of the "broken" crest heights in the probability domain.

To summarise these results and present them in a more consistent form, Figure 6 presents error contours similar to the investigation of wave heights (Figure 3). In this case, the errors [Eq. (12)] between the Forristall model [Eq. (11)] and the measured data for (a) the bulk (P_{20}) and (b) the tail (P_1) of the distribution are compared. In both sub-plots it is apparent that the Forristall model can describe moderate sea-states ($1 < H_s < 3$) with reasonable accuracy. However, as steeper sea-states are considered, significant departures between model and data arise. These are expressed both as nonlinear amplifications for sea-states in which there is not significant wave breaking, and as noteworthy reductions due to wave breaking in the steepest sea-states. Whilst these arise in both sub-plots, the magnitude of the deviations is arguably more pronounced in the tail of the distribution (Figure 6(b)). This is not unexpected since both effects will first affect the largest crest heights before progressing to larger probabilities of exceedance. Additionally, some discrepancies can be observed in even the most moderate sea-states ($H_s < 1$ m), typically for large peak periods. The most probable cause for these lies in some relative increase in the variability of the sea-state conditions included in the data bins. However, these conditions generally represent benign sea-states and have not been further investigated.

Regarding the distribution of normalised crest heights, it has been shown that the Forristall model can provide an accurate description of moderately steep sea-states. For steeper sea-states, the deviations observed can potentially lead to either an under-estimation (no/limited wave breaking) or an over-estimation (extensive wave breaking) of the largest crest heights in intermediate and shallow water depths. Further investigation of these effects has been presented in Karmpadakis (2019). This has been accompanied by additional evidence from other offshore platforms and an extensive experimental campaign.

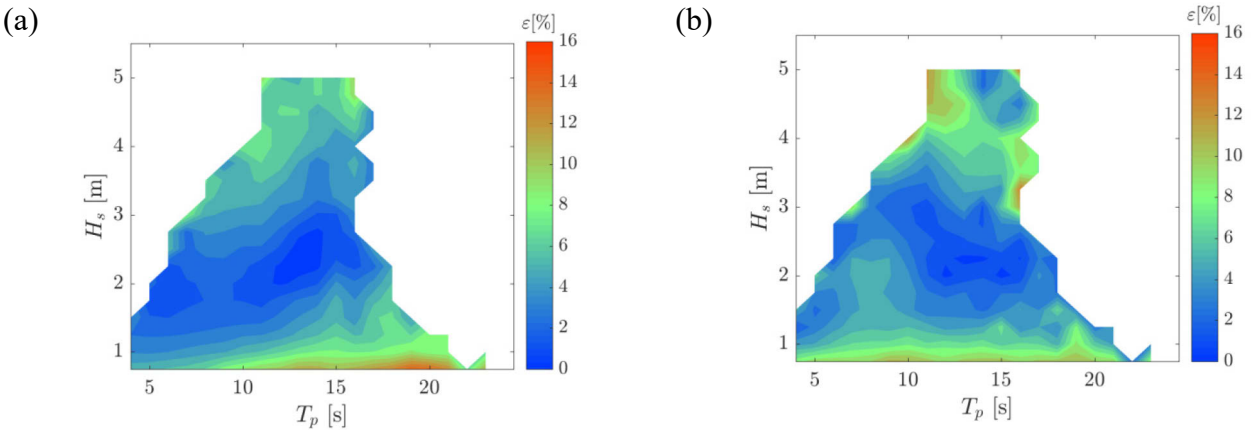

Fig. 6. Error contours comparing the available field data recorded in $d = 8$ m and the predictions of the Forristall model for (a) the bulk of the distribution - P_{20} [20%] probability level and (b) the tail of the distribution - P_1 [1%] probability level.

5 Conclusions

The analysis of a new dataset of field measurements has been presented. The data have been recorded using a wave radar mounted on an offshore platform and comply with the highest quality standards for offshore measurements. The analysis conducted herein has focused on the short-term distributions of wave heights and crest heights arising in a variety of sea-state conditions. The accuracy of existing statistical models has been assessed and guidance provided as to the most appropriate models across the $(H_s/d, k_p d)$ domain. Moreover, the regions of significant error accumulation have been indicated for the most commonly applied models and insights regarding the influence of key physical mechanisms provided. Taken together the results presented herein can be used for the derivation of appropriate design conditions for a variety of marine structures.

Acknowledgements

The authors would like to thank Shell for providing the data presented in this study. Additionally, the authors are grateful to the partners of the LoWiSh Joint Industry Project for funding this research.

References

Aqua, R. (2014) *WaveRadar REX Manual*, *Manual*.

Battjes, J. A. and Groenendijk, H. W. (2000) 'Wave height distributions on shallow foreshores', *Coastal Engineering*, 40(3), pp. 161–182. doi: 10.1016/S0378-3839(00)00007-7.

Battjes, J. A. and Janssen, J. P. F. M. (1978) 'Energy Loss and Set-Up Due to Breaking of Random Waves', *Coastal Engineering Proceedings*, 1(16), pp. 569–587. doi: 10.1061/9780872621909.034.

Boccotti, P. (1989) 'On mechanics of irregular gravity waves', *Atti della ASccad. naz. dei Lincei; A 386. Memorie/Classe di scienze fis., mat. e naturali.*, 19(VIII), pp. 111–170.

Christou, M. and Ewans, K. (2011) 'Examining a comprehensive dataset containing thousands of freak wave events. Part 2 - Analysis and findings', in *Proceedings of the ASME 30th 2011 International Conference on Ocean, Offshore and Arctic Engineering*. doi: 10.1115/OMAE2011-50169.

DNV (2010) *DNV-RP-C205 Environmental Conditions and Environmental Loads*, *Det Norske Veritas*.

Ewans, K., Feld, G. and Jonathan, P. (2014) 'On wave radar measurement', *Ocean Dynamics*, (64), pp. 1281–1303. doi: 10.1007/s10236-014-0742-5.

Forristall, G. Z. (1978) 'On the statistical distribution of wave heights in a storm', *Journal of Geophysical Research*, 83(C5), p. 2353. doi: 10.1029/JC083iC05p02353.

Forristall, G. Z. (2000) 'Wave Crest Distributions: Observations and Second-Order Theory', *Journal of Physical Oceanography*, 30(8), pp. 1931–1943. doi: 10.1175/1520-0485(2000)030<1931:WCDOAS>2.0.CO;2.

Glukhovskiy, B. (1966) 'Investigation of sea wind waves (in Russian)', in *Leningrad, Gidrometeoizdat (reference obtained from Bouws, E. 1979: Spectra of extreme wave conditions in the Southern North Sea considering the influence of water depth. Proc. of Sea Climatology Conference, Paris: 51-71)*.

Karmpadakis, I. (2019) *Wave Statistics in Intermediate and Shallow Water Depths*. Imperial College London.

Karmpadakis, I., Swan, C. and Christou, M. (2019) 'Laboratory investigation of crest height statistics in intermediate water depths', *Proceedings of the Royal Society A: Mathematical, Physical and Engineering Science*.(submitted)

Klopman, G. (1996) *Extreme wave heights in shallow water*.

Latheef, M. and Swan, C. (2013) 'A laboratory study of wave crest statistics and the role of directional spreading', *Proceedings of the Royal Society A: Mathematical, Physical and Engineering Sciences*, 469(2152), pp. 20120696–20120696. doi: 10.1098/rspa.2012.0696.

Longuet-Higgins, M. S. (1952) 'On the Statistical Distribution Of Sea Waves', *Journal of Marine Research*, 11(3), pp. 245–266.

Mai, S., Wilhelmi, J. and Barjenbruch, U. (2011) 'Wave height distribution in shallow waters', in *Coastal Engineering Proceedings*, p. 63. doi: 10.1016/0029-8018(85)90070-8.

Mendez, F. J., Losada, I. J. and Medina, R. (2004) 'Transformation model of wave height distribution on planar beaches', *Coastal Engineering*, 50(3), pp. 97–115. doi: 10.1016/j.coastaleng.2003.09.005.

Naess, A. (1985) 'On the distribution of crest to trough wave heights', *Ocean Engineering*, 12(3), pp. 221–234. doi: 10.1016/0029-8018(85)90014-9.

Sharma, J. and Dean, R. G. G. (1981) 'Second-Order Directional Seas and Associated Wave Forces', *Society of Petroleum Engineers Journal*, 21(1), pp. 129–140. doi: 10.2118/8584-PA.

Tayfun, M. A. and Fedele, F. (2007) 'Wave-height distributions and nonlinear effects', *Ocean Engineering*, 34(11–12), pp. 1631–1649. doi: 10.1016/j.oceaneng.2006.11.006.

van Vledder (1991) 'Modification of Glukhovskiy distribution - Southern North Sea Group Annex 2'.